Solid State Ionics 57 (1992) 91–98
North-Holland

SOLID
STATE
IONICS

Mixed conductivity in terbia-stabilized bismuth oxide

I.C. Vinke, B.A. Boukamp, K.J. de Vries [1] and A.J. Burggraaf
Laboratory for Inorganic Chemistry, Materials Science and Catalysis, Department of Chemical Technology, University of Twente, P.O. Box 217, 7500 AE Enschede, The Netherlands

Received 22 August 1991; accepted for publication 4 March 1992

The mixed conducting solid solution $0.75Bi_2O_3$–$0.25Tb_4O_7$ (BT40) was studied by impedance techniques using ionically blocking electrodes. These measurements confirmed the *p*-type electronic conductivity suggested in literature. In air at temperatures between 600 and 900 K the ionic transference number ranges from 0.28 to 0.70. The total conductivity at 833 K in air is 0.93 Ω^{-1} m^{-1}. The activation enthalpy for the electronic conductivity varies from 77 kJ/mol in pure O_2 to 83 kJ/mol in an ambient with $P_{O_2} = 2 \times 10^{-4}$ atm. The electronic conductivity seems to be a function of the sample geometry and increases with decreasing cross section to height ratio. The activation enthalpy for the ionic conductivity being 110 kJ/mol, is independent of the P_{O_2} and does not depend on the sample geometry.

1. Introduction

Bismuth oxide based mixed conducting ceramics are potentially interesting as electrode materials and semi-permeable membranes for use in electro-catalytic and permeation reactors. The materials system terbium oxide–bismuth oxide has already been studied by a number of authors with respect to the phase composition [1–3], the conductivity [1–3,4,5], the stoichiometry, i.e. the ratio of Tb^{3+}/Tb^{4+} [6], and the oxygen permeation [7].

From the phase studies it follows that in the solid solution with the composition 75 mol% Bi_2O_3–25 mol% Tb_4O_7, i.e. $Bi_{1.2}Tb_{0.8}O_{3-y}$ (BT40) the high temperature fcc structure is stable down to room temperature. The total conductivity (0.7 S cm^{-1} at 800 K [5]) is close to the conductivity of δ-Bi_2O_3. The conductivity data and transference number data presented by several authors, however, scatter considerably. Furthermore data on the ionic and electronic conductivity as a function of oxygen partial pressure are scarce [2]. These data are especially important for the understanding of the oxygen permeation properties of a mixed conductor.

The lack of reliable data has prompted us to investigate the conductivity of BT40 as a function of oxygen partial pressure, temperature and sample geometry and to relate these results with oxygen permeation data on Bi_2O_3–M_2O_3 solid solutions with M = Tb, Y or Er. Instead of using the concentration cell method for measuring the transference number, a method involving frequency dispersion measurements on samples with ionically blocking electrodes is used.

2. Experimental

The solid solution of bismuth oxide and terbium oxide was prepared using the co-precipitation method as described for erbia stabilized bismuth oxides by Kruidhof et al. [8]. Stoichiometric amounts of high purity Bi_2O_3 and Tb_4O_7 were dissolved in concentrated nitric acid. This solution was slowly added to a 4M ammonia solution. The precipitate was filtered and rinsed with distilled water. The precipitate was then dried in a furnace at 350 K, ball milled and calcined for at least eight hours at 1023 K. After cooling the powder was wet milled in acetone in a satellite mill for eight hours and was subsequently dried in air. The dried powder was first uniaxially and then isostatically pressed into boules. These boules were

[1] Author to whom all correspondence should by addressed.

placed in a crucible on a layer of their own powder and sintered for 16 h at 1143 K. This method prevents preferential evaporation from the boule as the atmosphere is in equilibrium with the surface of the boule.

The furnace was heated and cooled at a rate of 1 °/min. The density of the boules after sintering is better than 98% of the theoretical density ($\rho_{th}=8.69\times10^3$ kg/m^3) as calculated from XRD data.

After sintering, cylindrical samples with various cross sections to height ratios were cut from the boules (see table 1). Both faces of these samples were polished with 0.05 μm Al_2O_3 powder. Subsequently both faces of the samples were covered with a 1–2 μm thick gold layer first by dc-sputtering and followed by vacuum deposition. Special precautions were taken to prevent the gold from covering the side walls of the samples. The samples were annealed for one hour at 1143 K. The heating and cooling rate of the furnace was again 1 °/min. The annealed electrodes were inspected by SEM. The gold layers did not show porosity aside from an occasional pinhole. The gold electrodes are assumed to be sufficiently gas tight to create an ionically blocking electrode.

The sample was placed between two spring-loaded circular gold contacts of 10 mm ϕ in a furnace with a controlled and constant atmosphere.

The frequency dispersion of all samples was measured as a function of temperature in air. For sample A the dispersion was also measured as a function of P_{O_2}. Impedance measurements were performed using a Solartron 1255 FRA. The schematic setup is presented in fig. 1. The 50 Ω resistor functions as a pull up resistor for the signal generator. R_m is the measuring resistor. The measurements were performed at constant temperature and P_{O_2}. The signal amplitude was 10 mV peak–peak.

In nitrogen ($P_{O_2}=2\times10^{-4}$ atm.) frequency dispersion was observed for sample A. The dc resistance ($Z(\omega)_{\omega\to0}$), however, could not be determined from the dispersion (see fig. 3). In these cases the dc resistance of the sample was established by applying a dc potential of 10 mV across the sample. After sufficiently long waiting times to ensure steady state conditions the current was measured. The experiment was repeated with the potential reversed to eliminate influences of bias on the measurement. R_{dc} was obtained from the slope of the current–voltage data sets.

Table 1
Geometry data for the BT40 samples.

Sample	ϕ (mm)	h (mm)	Cross section/height ratio (mm)
A	10.0	1.5	52.4
B	7.82	1.43	33.6
C	7.82	4.55	10.6

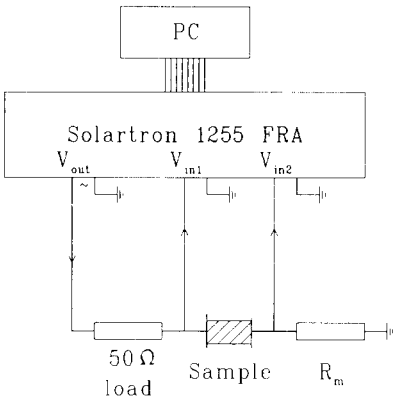

Fig. 1. Connection scheme for impedance measurements in a two electrode cell.

All measured resistances were converted to specific conductivities. These are obtained by multiplying the conductance by the sample thickness and dividing by the electrode surface area.

2.1. Impedance interpretation and analysis

In the temperature range studied the bulk resistance of BT40 is small enough so that no bulk dispersion due to the dielectric constant of the sample is observed in the frequency range used. All dispersions measured relate to the electrode process. The impedance of the Au | BT40 | Au cell is schematically represented by the idealized equivalent circuit of fig. 2 in which the bulk dispersion is represented by R_i only. Here the treatment for terbium–gadolinium zirconate proposed by Van Dijk et al. [9] is followed. R_{ct} represents the charge transfer resistance and C_{dl} the double layer capacitance of the electrode. R_i represents the ionic and R_e the electronic conductivity of the bulk. Eq. (1) expresses the fre-

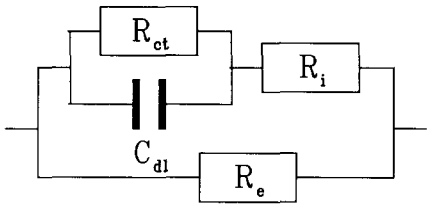

Fig. 2. Idealized schematic representation of the elements contributing to the impedance spectrum.

quency dependence of the impedance for the equivalent circuit of fig. 2:

$$Z(\omega) = \cfrac{1}{\cfrac{1}{\cfrac{1}{\cfrac{1}{j\omega C_{dl} + \cfrac{1}{R_{ct}}} + R_i} + \cfrac{1}{R_e}}}$$

$$= \frac{R_e(R_{ct} + R_i(1 + j\omega C_{dl} R_{ct}))}{(R_i + R_e)(1 + j\omega C_{dl} R_{ct}) + R_{ct}} . \qquad (1)$$

As the dense gold electrodes are assumed to be ionically blocking, R_{ct} may be assumed to be large in comparison with R_e and R_i. If R_e is much smaller than R_i no dispersion will be observed and the measured, frequency independent, impedance (resistance), will be equal to R_e.

If R_i and R_e are of the same order of magnitude, dispersion due to the double layer capacitance can be observed. Ideally this dispersion results in a semicircle in the Nyquist impedance plane. The low frequency intercept with the real axis (dc limit, R_{dc}) then represents the electronic resistance and is given in eq. (2a):

$$\frac{1}{R_{dc}} = \frac{1}{R_e} + \frac{1}{R_i + R_{ct}} \approx \frac{1}{R_e} . \qquad (2a)$$

The high frequency intercept (for $\omega \to \infty$), R_∞, is then given by

$$\frac{1}{R_\infty} = \frac{1}{R_e} + \frac{1}{R_i} . \qquad (2b)$$

Whether dispersion is observed depends on the value of C_{dl}. If ωC_{dl} is large with respect to $(R_{ct})^{-1}$ in the frequency range used this capacitance will form a short circuit and the measured (dispersionless) impedance will be equal to R_∞ (eq. (2b)). On the other hand if ωC_{dl} is small with respect to $(R_{ct})^{-1}$ in the frequency range used the ionic branch of the equivalent circuit will be blocked completely (note: $R_{ct} \to \infty$). The measured (dispersionless) resistance will then be equal to the electronic resistance.

3. Results

3.1. Influence of the oxygen partial pressure

At high P_{O_2} values no dispersion was observed. Only in nitrogen ($P_{O_2} = 2 \times 10^{-4}$ atm) the impedance measurements showed a clear dispersion. A few examples of these are presented in the Nyquist diagrams of fig. 3. The observed dispersion suggests the presence of a (semi-infinite) diffusion process (Warburg). This Warburg may be attributed to diffusion of oxygen in the electrode/electrolyte interface as, with respect to the ambient, a gradient is created in the oxygen activity under influence of the ac potential. The Warburg is assumed to be parallel to the ideal double layer capacitance. Effectively it may replace this capacitance. The Warburg diffusion effect, however, will not be considered in this study.

Fig. 4 presents the specific conductivity values obtained from the (frequency independent) resistances for $P_{O_2} > 2 \times 10^{-4}$ atm and from the high frequency intercepts with the real axis in the Nyquist diagram for $P_{O_2} = 2 \times 10^{-4}$ atm (nitrogen). For the measurements at $P_{O_2} = 2 \times 10^{-4}$ atm the dc conductivity is also presented in this graph (line 4). The curves of R_∞ in fig. 4 for $P_{O_2} = 1.0$ atm (line 1) and $P_{O_2} = 0.21$ atm (line 2) are not straight lines suggesting that R_∞ is the sum of two temperature activated processes.

From the ac and dc measurements at $P_{O_2} = 2 \times 10^{-4}$ atm the ionic and electronic conductivity can be obtained using eqs. (2a) and (2b). In fig. 5 the resulting electronic conductivity (line 3) and ionic conductivity (line 4) are presented.

The high ionic conductivity of bismuth oxide based (mixed) conductors is due to the large concentration of empty oxygen lattice sites (mobile oxygen

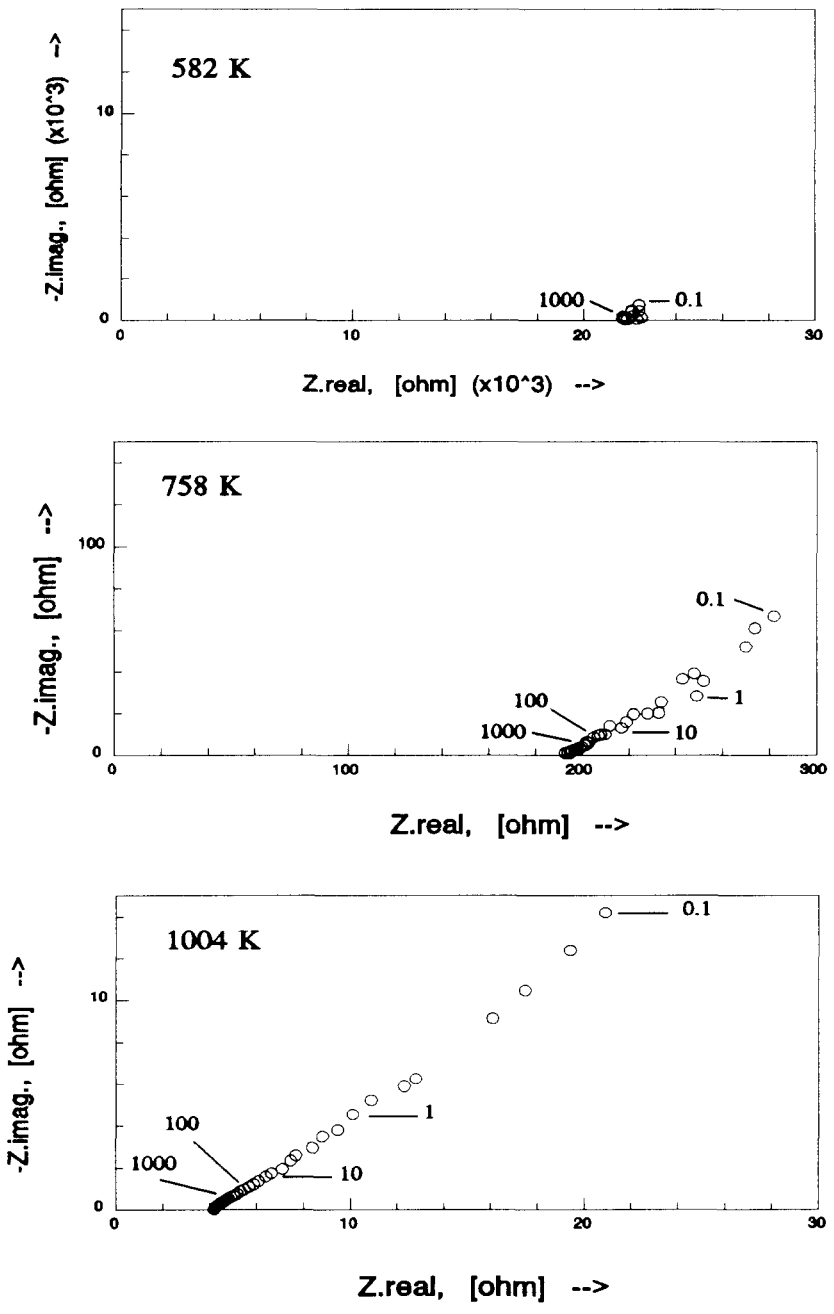

Fig. 3. Examples of frequency dispersion data for BT40 at $P_{O_2} = 2 \times 10^{-4}$ atm. Numbers in the graph represent the frequency in Hz.

"vacancies") in the defect fluorite structure [10]. The equilibrium of BT40 with the atmosphere is described by eq. (3):

$$4Tb_{Tb}^{\times} + 2V_{O}^{\cdot\cdot} + O_{2,g} \rightleftarrows 4Tb_{Tb}^{\cdot} + 2O_{O}^{\times}, \quad (3)$$

with $4Tb_{Tb}^{\cdot} \equiv 4h^{\cdot}$.

The total concentration of oxygen vacancies will not

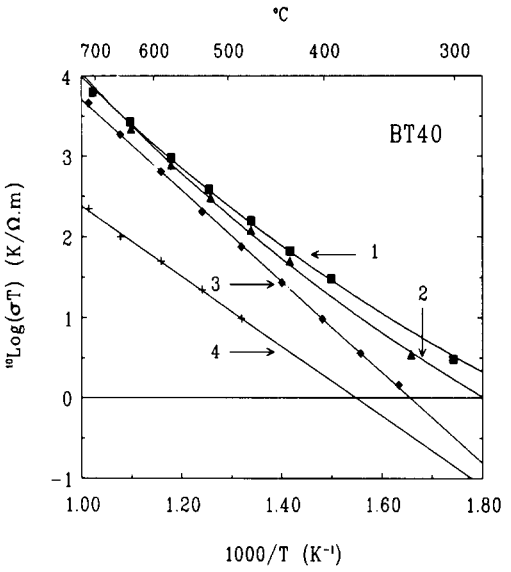

Fig. 4. High frequency intercept σ_∞ from the impedance data for BT40: (1) oxygen (■); (2) air (▲); (3) nitrogen (♦) and (4) σ_{dc} for nitrogen (+).

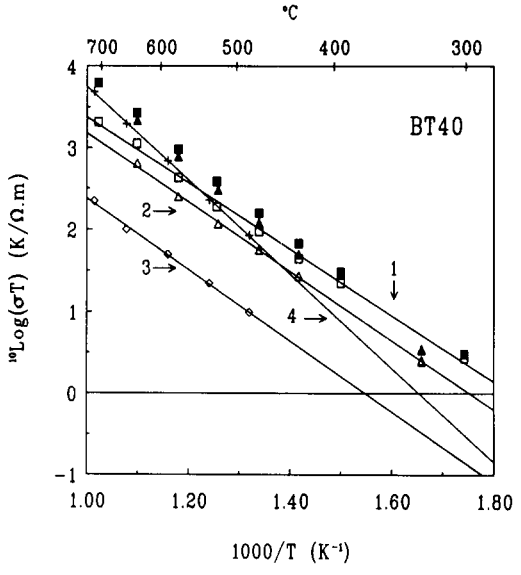

Fig. 5. Electronic ((□) oxygen, (△) air, (◇) nitrogen) and ionic conductivity (+) as calculated for BT40. Closed symbols represent the total conductivity σ_∞.

be influenced noticably by a shift in the equilibrium of eq. (3). Hence the ionic conductivity is expected to be virtually independent of P_{O_2}. Using this assumption and eq. (2b) we can calculate the actual electronic conductivity for $P_{O_2}=1.0$ atm and $P_{O_2}=0.21$ atm. The results of these calculations are also presented in fig. 5 (line 1 and line 2 respectively). For comparison the total conductivity values obtained from R_∞ as measured in oxygen and air are added (closed symbols).

The activation enthalpies for the electronic conductivities and the ionic conductivity, obtained from the slopes of the lines in fig. 5, are presented in table 2.

From fig. 5 we see that in oxygen and air, at low temperatures, R_∞ is dominated by the electronic conductivity, i.e. the total conductivity is mainly electronic. In the high temperature region R_∞ shifts to predominantly ionic conductivity. This means that although no dispersion is observed, the value of R_∞ is not equal to the dc conductivity, contrary to what was assumed in the previous paragraph. In nitrogen atmosphere the total conductivity is mainly ionic.

This is also expressed by the ionic transference numbers that can be calculated from the R_e and R_i, which are presented in fig. 6 together with some data from literature. The transference number measurements agree with the data of Esaka et al. [2] who obtained their data using the concentration cell method (low $P_{O_2}=0.21$ atm, high $P_{O_2}=1.0$ atm).

3.2. Influence of the sample geometry

Frequency dispersion measurements on the samples B and C in air yielded impedance spectra that are comparable with the results obtained for sample A. The data were therefore treated similar as described above. In fig. 7 the total conductivity for all three samples (A, B and C) is represented by the closed symbols. As we already have noted for the

Table 2
Activation enthalpies for the lines given fig. 5.

Activation enthalpies for BT40		
P_{O_2} (atm)	ΔH_e (kJ/mol)	ΔH_i (kJ/mol)
1.0	77±2	110±1
0.21	81±1	110±1
2×10^{-4}	83±2	110±1

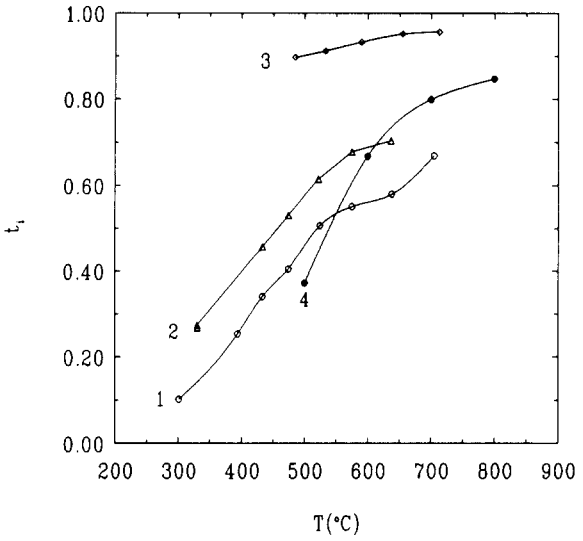

Fig. 6. Ionic transference numbers for BT40 as a function of temperature and P_{O_2}; (1) $P_{O_2}=1.0$ atm; (2) $P_{O_2}=0.21$ atm; (3) $P_{O_2}=0.002$ atm; (4) $P_{O_2}=0.21$ atm. (1)-(3) this work, (4) Esaka et al. [2].

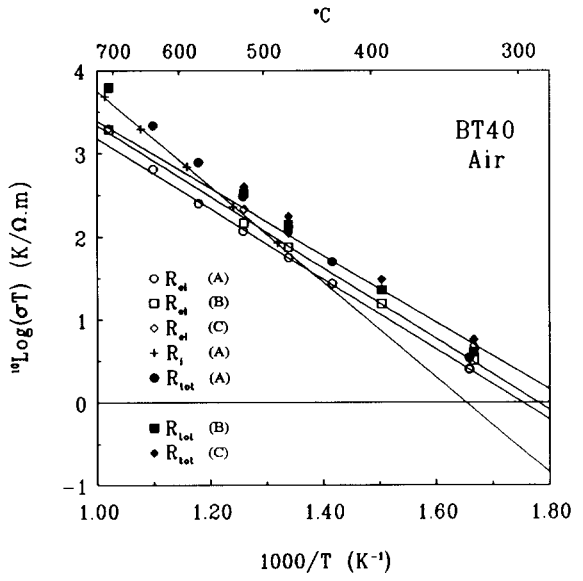

Fig. 7. Total (closed symbols), ionic (+) and electronic conductivity (open symbols) for BT40 for different cross section to height ratios (table 1) as a function of temperature measured in air.

measurements as a function of the oxygen partial pressure, the data points lie on curves that can be described using the sum of two exponential equations. The data for different sample geometries are equal at high temperatures. At lower temperatures the total conductivity values seem to increase with the cross section to height (S/h) ratio.

Because the high temperature data do not vary with the geometry and as it was shown above, that at these temperatures the total conductivity is determined by the ionic conductivity, we assume that the *ionic* conductivity is not a function of the sample geometry. Subtracting these ionic conductivity values from the total conductivity results in the electronic conductivity values as presented in by the open symbols in fig. 7.

From this figure it can be concluded that the electronic conductivity is a function of the sample geometry and decreases with increasing S/h ratio. The activation enthalpy of the electronic conductivity however remains constant.

4. Discussion

To check the result of the conductivity measurements a comparison with literature results is made. In table 3 a list of activation enthalpies for ionic and electronic conductivities as found in literature is given. All values in this table are obtained at $P_{O_2}=0.21$ atm. The activation enthalpies for the R_e and R_i from this work are comparable with the values from literature (note that the activation enthalpies from literature are recalculated for a $^{10}\log(\sigma T)$ scale). A comparison of the specific total conductiv-

Table 3
Total conductivity at $T=833$ K and activation enthalpy for the ionic and electronic conductivities of BT40 in air.

Conductivity data on BT40			
Electronic	Ionic		
ΔH (kJ/mol)	ΔH (kJ/mol)	σ_{833} (Ω^{-1} m^{-1})	Ref.
63	119	7.8×10^{-1}	[2]
84	118	9.1×10^{-1}	[5]
81	110	9.3×10^{-1}	this work

ity values is made at 833 K. As shown in table 3, the values for our measurements in air are in agreement with values reported in literature.

The slopes for the P_{O_2} dependence of the electronic conductivity in fig. 8 are close to 0.25. The electronic conductivity can thus be discribed by:

$$\sigma_e(T, P_{O_2}) = k \exp\left(\frac{-\Delta H}{RT}\right)(P_{O_2})^n ,$$

with $n \approx \frac{1}{4}$. (4)

This $(P_{O_2})^{1/4}$ dependency for the electronic conductivity is generally observed for electron–hole conductors, indicating that BT40 is a *p*-type mixed conductor. Hence the equilibrium with the gas phase is accurately described by eq. (3). From eq. (4) it is obvious that if the P_{O_2} decreases the hole conductivity will decrease too due to a decrease in the electron–hole concentration, i.e. a decrease in the Tb^{4+} concentration. From XAS measurements on rapidly quenched samples, equilibrated at 872 K in air, van der Laan et al. [6] found that only 5% of the terbium ions was in the Tb^{4+} state. With constant temperature and decreasing P_{O_2} the ionic transference number will therefore approach 1.0.

This P_{O_2} dependence of the electronic conductivity has important consequences for the permeation of oxygen through dense ceramic samples of BT40. BT40 will become mainly an ionic conductor at low P_{O_2} values ($t_i \rightarrow 1.0$) hence the permeation measured with a gradient in which P_{O_2} values occur lower than 2×10^{-4} atm will be considerably smaller than can be expected from the average conductivity data published until now. This mainly ionic conducting zone will behave like a solid electrolyte and the permeation will be determined by the value of the σ_e *in this zone* (Wagner theory) which is considerably smaller than the average value.

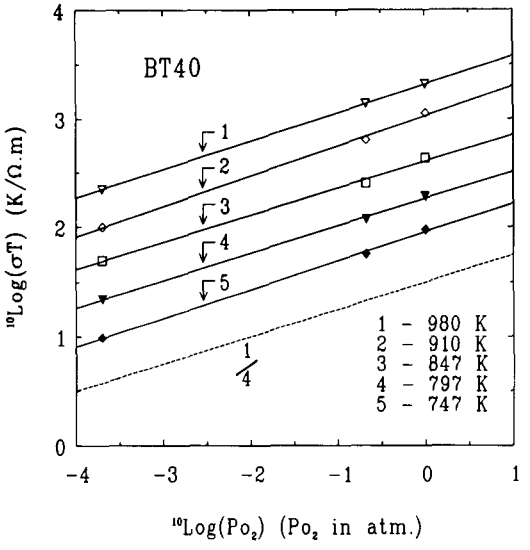

Fig. 8. The electronic conductivity of BT40 as a function of P_{O_2}. The dashed line represents a slope of 1/4.

The results of the conductivity measurements as a function of sample geometry show a dependence on the geometry for the electronic conductivity. This indicates that an extra contribution to the electronic conductivity must be present. This extra contribution cannot however simply be explained by a surface conductivity because it can be shown that for the samples B and C the influence of the difference in geometry is equal for the bulk and the surface conductivity, i.e. a difference in electronic conductivity cannot arise from surface conductivity.

An explanation for this observed phenomenon can not be given at this point.

5. Conclusions

BT40 is a *p*-type mixed conductor.

The activation enthalpy for the electronic conductivity varies slightly with P_{O_2} between 77 kJ/mol in pure oxygen to 83 kJ/mol for nitrogen ($P_{O_2} = 2 \times 10^{-4}$ atm).

At low P_{O_2} the ionic transference number approaches the value 1.

The electronic conductivity seems to vary with the cross section over height ratio.

The measurement of the ionic and electronic conductivity using blocking electrodes is likely to produce results that are more accurate than data obtained by the concentration cell method.

Acknowledgement

The research presented in this publication was supported by the Netherlands Foundation for Chemical Research (SON) with financial aid from the

Netherlands Organisation for Scientific Research (ZWO).

References

[1] H.T. Cahen, T.G.M. van de Belt, J.H.W. de Wit and G.H.J. Broers, Solid State Ionics 1 (1980) 411.
[2] T. Esaka and H. Iwahara, J. Appl. Electrochem. 15 (1985) 447.
[3] P. Shuk, S. Jacobs and H.H. Möbius, Z. Anorg. Allg. Chem. 524 (1985) 144.
[4] P.P. Shuk, A.A. Vecher and V.V. Samochval, Thermochim. Acta 93 (1985) 461.
[5] B.A. Boukamp, M.P. van Dijk, K.J. de Vries and A.J. Burggraaf, in: Nonstoichiometric Compounds, eds. C.R.A. Catlow and W. Mackrodt, Advances in Ceramics, Vol. 23 (1987) 447.
[6] G. van der Laan, J.C. Fuggle, M.P. van Dijk, A.J. Burggraaf, J.M. Esteva and P. Karnatak, J. Phys. Chem. Solids 47 (1986) 413.
[7] H.J.M. Bouwmeester, to be published.
[8] H. Kruidhof, K. Seshan, B.G. Lippens Jr., P.J. Gellings and A.J. Burggraaf, Mat. Res. Bull. 22 (1987) 1635.
[9] M.P. van Dijk, K.J. de Vries and A.J. Burggraaf, Solid State Ionics 16 (1985) 211.
[10] I.C. Vinke, Electrochemical and electrode properties of stabilized bismuth oxide ceramics, Ph.D. Theses (University of Twente, 1991) Chapt. 2.